Journal of Metals, Materials and Minerals, 34(2), 1804, 2024

The effect of printing parameters on the properties of 17-4 PH stainless steel fabricated by material extrusion additive manufacturing

Phanuphak SEENSATTAYAWONG[1], Chanun SUWANPREECHA[1,*], Natthanicha BOONLERT[1], Sukrit SONGKUEA[1], and Anchalee MANONUKUL[1,*]

[1] *National Metal and Materials Technology Center (MTEC), National Sciences and Technology Development Agency (NSTDA), 111 Thailand Science Park, Klong Luang, Pathumthani 12120, Thailand*

***Corresponding author e-mail**: anchalm@mtec.or.th, chanun.suw@mtec.or.th

Received date:
9 August 2023
Revised date
4 March 2024
Accepted date:
3 April 2024

Keywords:
Additive manufacturing;
Printing parameter;
17-4PH;
Sintering;
Density

Abstract

The 17-4PH stainless steel filament was characterised and utilised to study the effect of printing parameters, i.e. printing temperature, layer thickness, infill pattern and extrusion multiplier on the physical properties. The as-printed and as-sintered internal structures were analysed. The results showed that the as-printed density increases with increasing printing temperature and extrusion multiplier and decreasing layer thickness. The use of the line infill pattern also provided slightly higher as-printed density than the concentric infill pattern due to the low fraction of void between deposited paths. After sintering, the trace of these voids can be observed together with smaller-size residual pores from the spaces between powders, which is the nature of the pressureless sintering process. The microstructure of the as-sintered specimens was similar to the typical microstructure of the 17-4PH alloy fabricated by metal injection moulding process, which contains delta ferrite, martensite and Si-rich phases. In additions, the internal void generated during debinding and sintering results in unexpectedly low tensile properties and results in the difference in tensile properties between the concentric and line infill patterns.

1. Introduction

Metal additive manufacturing (AM) has been widely studied and utilised in various fields since it can fabricate various types of alloys [1-4] with almost unlimited shapes and a wide range of sizes depending on the printer's capability. The additive-manufactured parts also have high accuracy and excellent mechanical properties [3,5]. Among several types of metal AM, metal material extrusion (MEX) method using a metal-filled filament has received much interest during the last decade [6,7]. To fabricate MEX parts, there are two main steps, which are (i) printing and (ii) debinding and sintering [6,7]. For the printing step, a metal-filled filament, consisting of a mixture of metal powder and polymeric binders, is heated and then extruded through a printer nozzle onto the printing bed layer by layer following and controlled by a computational 3D design. Subsequently, the printed parts will be debound and sintered, during which the debinding method depends on the binder used and the sintering temperature and time depend on the metal powder, reminding binder and their relative content. Therefore, MEX does not need to deal with loose powder and there is no need for high-power sources as used in selective laser melting (SLM) and electron beam melting (EBM), thus providing a safer and more economic route [8-10], even though the mechanical properties of the additively manufactured parts are slightly lower [9].

Until now, several studies have shown that MEX can fabricate several sinterable alloys such as 316L [9,11-14] and 17-4PH stainless steel [15-19], M2 tool steel [20], CP-Ti [21], bronze [22], Cu [23], Cu-12Si [24,25], Ti-6Al-4V [26-29], Inconel 625 [30] and Inconel 718 [31] by using in-house developed filaments, commercially available closed systems such as MetalX by Markforged Inc. or commercial metal-filled filaments such as Ultrafuse 316L [32] and Filamet by the Virtual Foundry, Inc. [33]. Although these commercial filaments are supplied with advice on recommended printing, debinding and sintering parameters, the density and mechanical properties of the MEX parts can still be subject to significant variation depending on processing parameters, especially the printing and sintering parameters [7]. Several studies suggest that the printing process has an essential role in determining the as-sintered mechanical properties, and especially the as-printed density and the relative as-sintered density [10,27]. To achieve a high relative sintered density in MEX parts, the MEX parts should have high relative as-printed density [10,27].

The essential printing parameters that usually influence the as-printed properties and density are the printing temperature, the layer thickness and the extrusion multiplier [10,13,24,25,27,34-37]. It was reported that a higher printing temperature provides higher as-printed tensile properties [10]. However, an excessively high printing temperature significantly generates high residual stress, thus leading to warpage defects [34]. Regarding the effect of layer thickness, most studies reported that thinner layer thickness provides higher mechanical properties [13,35-37], since the voids between printing paths are reduced. However, as contradictorily reported by Godec *et al.*, a thicker layer thickness is said to provide better properties due to

the reduction of weak points between the printing paths [10]. On the other hand, Singh *et al.* [27] and Quarto *et al.* [13] reported that the variation in the layer thickness does not significantly influence density if sufficient binder is used together with sufficient control of the printing process. With respect to the extrusion multiplier, it was found that an increase in extrusion multiplier contributed to a significant increase in as-printed and as-sintered densities and as-printed tensile properties [10,27]. Moreover, it was also found that an increase in extrusion multiplier up to 1.2 can improve surface quality [37]. Nevertheless, a too high level for the extrusion multiplier may result in deformation of the printed parts because of excessive material [38]. It can be seen that the effects of varying printing parameters vary case by case, depending on the feedstock and printing process.

Therefore, the effect of printing parameters, which are the printing temperature (210°C, 220°C and 235°C), the layer thickness (0.1 mm, 0.2 mm, and 0.3 mm), the infill pattern (line and concentric) and the extrusion multiplier (1.35 and 2.0) on the as-printed properties, when using a commercially available 17-4PH metal-filled filament were analysed. The as-printed and related as-sintered internal structures of the parts printed with the most optimum condition were revealed through micro-computed tomography (micro-CT) scans. The as-sintered microstructure was also analysed through optical microscopy (OM), X-Ray Diffraction (XRD) and scanning electron microscopy (SEM).

2. Experimental procedures

2.1 Filament characterisation

The commercially available 2.75 mm 17-4PH stainless steel filament, supplied by the Virtual Foundry, Inc., was utilised as feedstock in this study. The binder characteristic and its fraction were analysed by Mettler Toredo thermogravimetric (TG) analysis with a heating rate of 10°C·min^{-1} from 30°C to 600°C under N_2 purging atmosphere with the rate of 10 mL·min^{-1}. The 17-4PH stainless steel powder morphology and its size and distribution were analysed using the remained powder from the TG analysis.

2.2 Specimen fabrication

The 17-4PH stainless steel filament was used to fabricate rectangular solid boxes with dimensions of 10 mm × 15 mm × 5 mm, as presented in Figure 1(a), using a desktop fused filament fabrication (FFF) printer (Ultimaker S5) through the Cura software. The overall printing parameters utilised in the present study are reported in Table 1. The top-view characteristic of line (also called grid or rectilinear) and concentric infill patterns with the corresponding as-printed and as-sintered specimens utilising these infill patterns are shown in Figure 1(b). The line infill pattern was alternated 90° between layers.

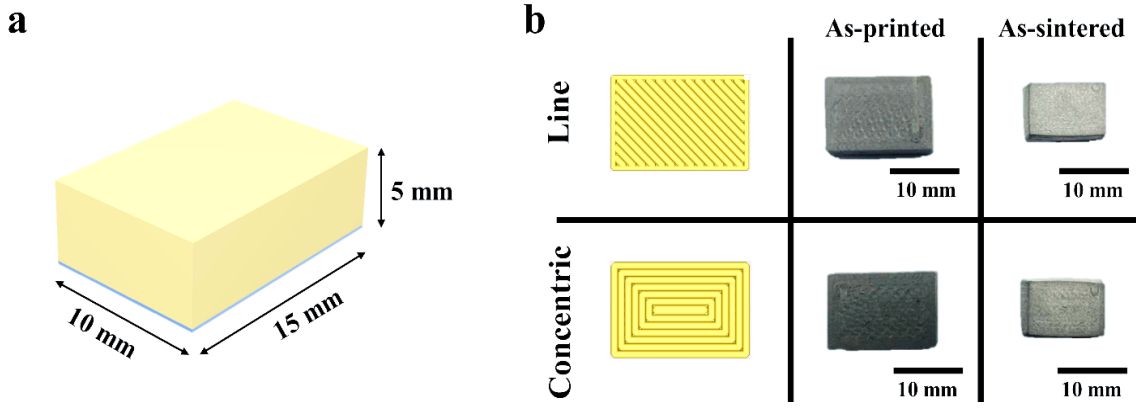

Figure 1. (a) Dimension of the as-printed solid box**,** and (b) characteristic of line and concentric infill patterns and corresponding as-printed and as-sintered specimens.

Table 1. Printing parameters.

Printing parameters		Details
Independent parameters	Layer thickness (mm)	0.1, 0.2, 0.3
	Printing temperature (°C)	210, 220, 235
	Infill pattern	Line (90° alternating), concentric
	Extrusion multiplier	1.35, 2.0
Fixed parameters	Wall line count	2
	Top/ bottom thickness (mm)	0.5
	Top/ bottom layer	1
	Infill density (%)	100
	Build plate temperature (°C)	60
	Printing speed (mm·s^{-1})	45
	Infill speed (mm·s^{-1})	45
	Wall speed (mm·s^{-1})	30
	Fan speed (%)	100

The independent printing parameters were layer thickness, printing temperature and infill pattern. Three specimens were fabricated and analysed in each parameter. The extrusion multiplier was varied after yielding the best printing parameters from those independent parameters based on the highest as-printed density. It is noted that the extrusion multiplier is the rate of the extruded materials, which is an adjustable parameter in the printer.

2.3 Debinding and sintering process

The thermal debinding heating profile was in-house optimised to ensure that all binders were completely removed based on the TG results. The thermal debinding was conducted in the N_2-flow atmosphere at the debinding temperature of 427°C for 3 h and 593°C for 2 h with the heating rate of 1.8°C·min^{-1}. After sintering, the samples were furnace cool under N_2-flow atmosphere. The effect of sintering temperature (1300°C, 1325°C and 1350°C) and time (1 h, 2 h and 4 h) was studied to determine the condition which yielded the highest relative sintered density, using as low sintering temperature and time as possible to avoid undesirable grain growth. The optimised sintering condition was found to be 1325°C for 2 h in an argon partial pressure atmosphere with a heating rate of 2.5°C·min^{-1} and this condition was used for the present study. The debinding and sintering were continuously conducted using a Shimadzu furnace (VHLgr20/20/23). Only the specimens that were printed with the condition providing the highest as-printed density were thermally debound and sintered for each infill pattern. The appearance of as-printed and as-sintered specimens prepared by the optimum printing, debinding and sintering conditions are shown in Figure 1(b).

2.4 Physical and microstructural characterisations

The apparent, as-printed, as-sintered densities and porosity were determined by the Archimedes' method [39], which can be calculated following Equation (1-4).

$$\text{Apparent density (g·m}^{-3}\text{)},\ \rho = m_{\text{in air}} \times \frac{\rho_{liquid}}{m_{in\ air} - m_{in\ liquid}} \qquad (1)$$

where ρ_{liquid} is the density of the liquid that generates buoyancy, $m_{in\ air}$ is the mass of the specimen measured in air, $m_{in\ liquid}$ is the mass of the specimen measured in liquid. Porosity of the as-printed specimen can be calculated following Equation (2).

$$\text{Porosity (\%)} = \left(1 - \frac{\rho_{as\text{-}printed}}{\rho_{theoretical\ as\text{-}printed}}\right) \times 100 \qquad (2)$$

where $\rho_{as\text{-}printed}$ is the apparent density of the as-printed specimen. $\rho_{theoretical\ as\text{-}printed}$ is the fully dense density of the as-printed part or filament, which can be calculated following Equation (3).

$$\rho_{theoretical\ as\text{-}printed} = \frac{100}{\%\ m_{powder}/\%\ \rho_{powder} + m_{binder}/\rho_{binder}} \qquad (3)$$

where $\%\ m_{powder}$ is the mass percentage of 17-4PH stainless steel powder in the filament and ρ_{powder} is the density of 17-4PH stainless steel powder, which is measured and averaged to be 7.90 ± 0.035 g·cm^{-3} and $\%\ m_{binder}$ is the mass percentage of binder in the filament and ρ_{binder} is the density of binder (1.24 g·cm^{-3} [40]). Relative sintered density can be calculated following Equation (4).

$$\text{Relative sintered density (\%)} = \frac{\rho_{as\text{-}sintered}}{\rho_{powder}} \times 100 \qquad (4)$$

where $\rho_{as\text{-}sintered}$ represents the apparent density of the as-sintered specimen.

The phase identification of powder after TG analysis and an as-sintered specimen was analysed, using an X-ray diffractometer (RIGAKU, TTRAX III), with Cu-Kα radiation. A step size of 0.05° at a scanning rate of 3°·min^{-1} was used. For microstructural observation, the as-sintered specimen was prepared by a standard metallographic method and then imaged by optical microscopy (Olympus-STM7) and field emission scanning electron microscopy (FE-SEM, JEOL JSM-7800F) equipped with EDS apparatus. To reveal the microstructure, the specimen was etched by using Glyceregia reagent (50 vol% HCl, 33 vol% Glycerol and 17 vol% HNO_3).

For internal structure analysis, a Nikon MCT 225 was utilised to perform micro-CT measurements with the parameters of 200 kV, 200 µA, 2 mm Cu filter, picture volume; 1200 images that generated 0.011 mm·voxel^{-1} of resolution. Only as-printed and as-sintered specimens that exhibited the highest density with the line and concentric infill patterns were analysed.

The tensile properties of as-sintered specimens were examined with the constant speed of 0.5 mm·min^{-1}, using a universal testing machine (Instron model 8872), equipped with a laser extensometer for strain measurement.

3. Results and discussion

3.1 Filament characteristics

A cross-sectional view of the metal filament is shown in Figure 2(a). The high magnification image of the filament in Figure 2(b), shows some rounded metal powders that are embedded in the binder matrix. No voids were observed over the inspected cross section of the filament. Figure 3 exhibits the TG result for the filament, showing the weight loss and the derivative of weight loss, in which the filament starts decomposing at 250°C and finishes at 500°C. It also reveals that there are at least two main components in the binder. The temperatures corresponding to the maximum decomposition rate of those binders are at 300°C and 400°C. These results were utilised for designing the debinding process. In addition, the filament contains a powder fraction of 77 wt% (35 vol%). As reported in Ref. [40], the binder in the filament mainly composes of Polylactic Acid (PLA), in which the density of 1.24 g·cm^{-3} for binder is used for a calculation of the theoretical density of the as-printed part. The theoretical density of as-printed part utilised in the present study is 3.54 g·cm^{-3}.

The metal powder after TG analysis, as shown in Figure 4(a), has a spherical shape with a small number of satellite particles, and is suitable for FFF fabrication [7]. Figure 4(b) shows the powder size and its distribution. The powder sizes are D_{10}: 27.78 µm, D_{50}: 31.99 µm and D_{90}: 46.79 µm. The largest powder size is at least two times smaller than the smallest layer thickness in the present study, confirming that the part can be fabricated with a layer thickness of 0.1 mm to 0.3 mm.

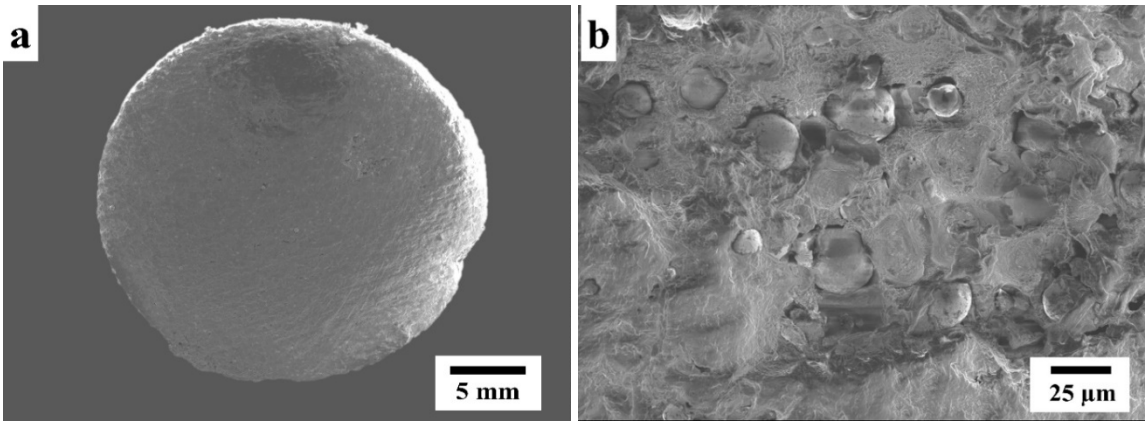

Figure 2. SEM images of (a) ground cross-sectional 17-4 PH stainless steel metal-filled filament, and (b) metal powder embedded and distributed in the polymer binder of the filament.

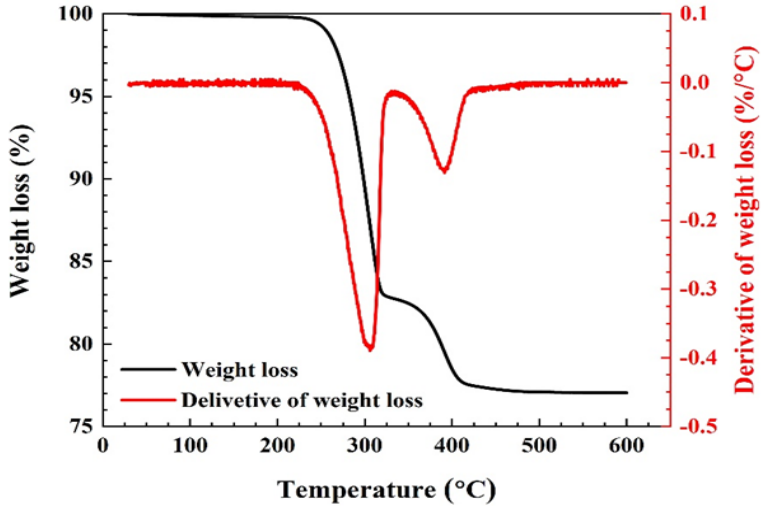

Figure 3. TG analysis of the 17-4 PH stainless steel metal-filled filament.

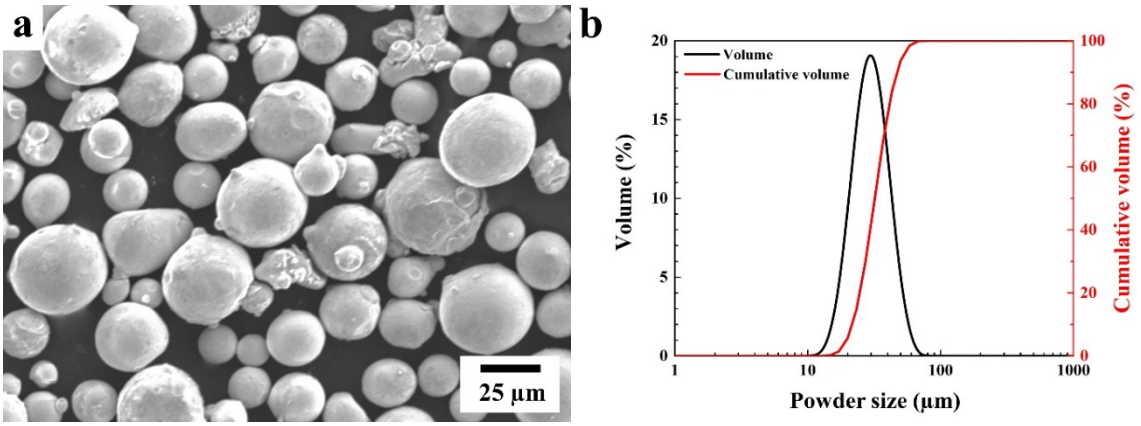

Figure 4. (a) Powder characteristic in the metal-filled filament, and (b) powder size distribution of the powder.

3.2 Influence of printing parameters on density

The effect of layer thickness and printing temperature on the as-printed density and porosity of specimens printed with the line and concentric infill patterns are shown in Figure 5(a-b). It was found that the layer thickness, printing temperature and infill patterns significantly affected the as-printed density and porosity. A decrease in layer thickness and an increase in printing temperature resulted in increasing as-printed density and decreasing porosity for both infill patterns in this work. These observations are in good agreement with the 17-4PH stainless steel MEX results reported by Godec *et al.* [10]. As the layer thickness decreases, the voids between deposited paths are reduced, thus increasing

the as-printed density. However, it is still unclear that why the as-printed density of specimens printed with the line infill pattern and with a layer thickness of 0.3 mm is higher than that of 0.2 mm. Considering the influence of printing temperature, for the line infill pattern, an increase of 10°C in the printing temperature from 210°C to 220°C provided a slight increase in density, while an increase of 15°C in the printing temperature from 220°C to 235°C provided relatively higher increment in density. Also, a similar trend of an increase in as-printed density and decrease in porosity with an increase in printing temperature can be observed with that of a concentric infill pattern. This behaviour can be explained through a decrease of feedstock viscosity with the higher printing temperature, which leads to a higher flow rate, smooth printing and filling between deposited paths, thus increasing density. Moreover, the use of a line infill pattern provided higher as-printed density than a concentric infill pattern. This behaviour will be discussed further in section 3.3.

Therefore, the printing parameters of 0.1 mm layer thickness and 235°C printing temperature, which provided the highest as-printed density for both infill patterns, were used as the optimum condition for further investigation.

The effect of the extrusion multiplier on the as-printed density and porosity of specimens printed with the optimum printing condition (0.1 mm layer thickness and 235°C printing temperature) for both infill patterns is presented in Figure 6. The results show that an increase in extrusion multiplier provides higher as-printed density and lower porosity for both infill patterns, which agrees well with other works [10,27]. Although Rosnitschek *et al*. [38] reported that too high extrusion multiplier may result in the deformation of the as-printed parts because of excess material, such deformation was not observed in the as-printed parts produced in the present study.

The as-printed and as-sintered densities of specimens printed under the optimum conditions for highest density are presented in Figure 7. Although the as-printed density of the specimen printed with the line infill pattern is 0.09 g·cm^{-3} higher than the concentric infill pattern, the as-sintered density of specimens printed by both line and concentric infill patterns are not significantly different.

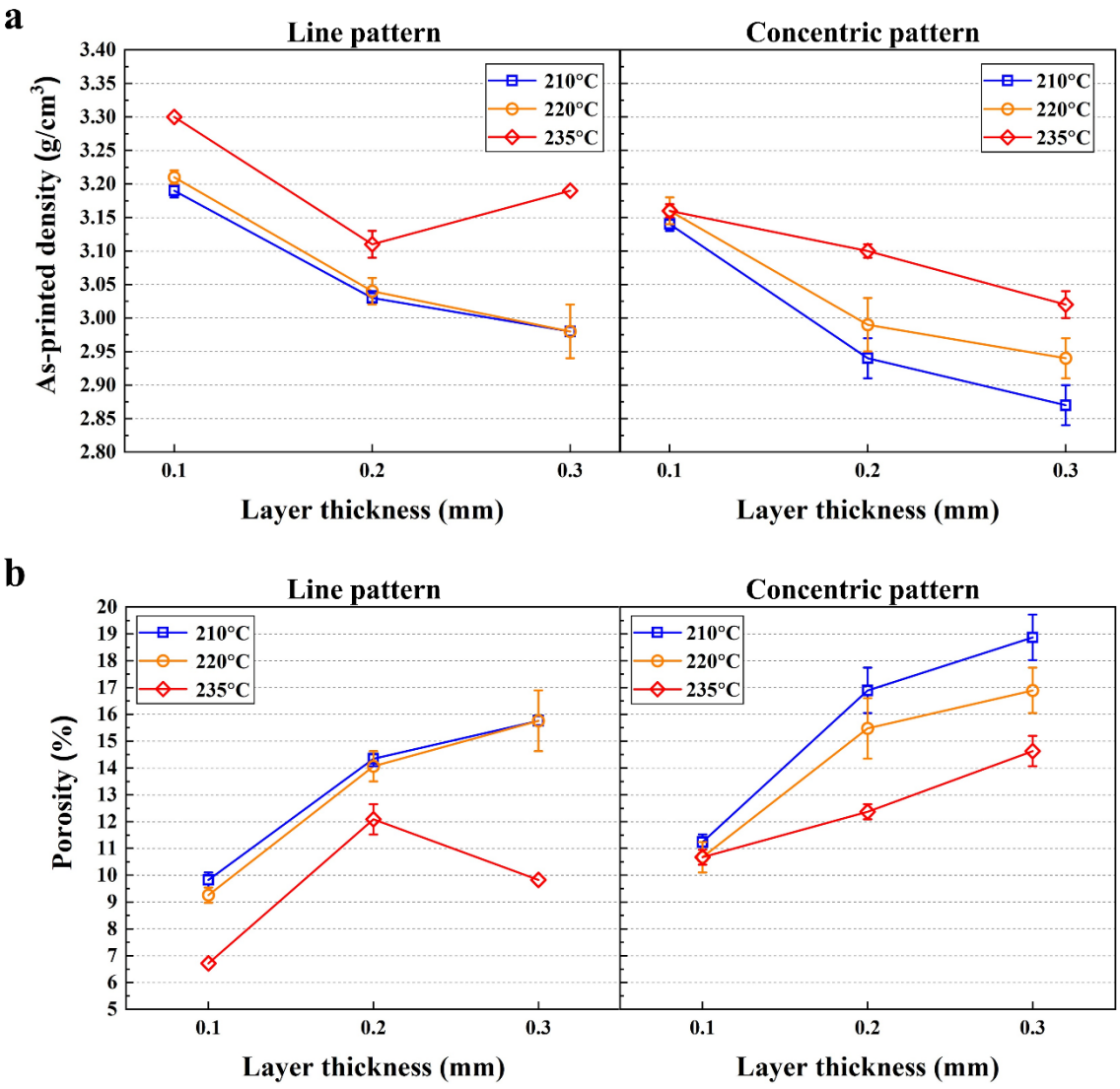

Figure 5. Effect of layer thickness and printing temperature on the (a) as-printed density of specimens, and (b) porosity printed with the line and concentric infill patterns.

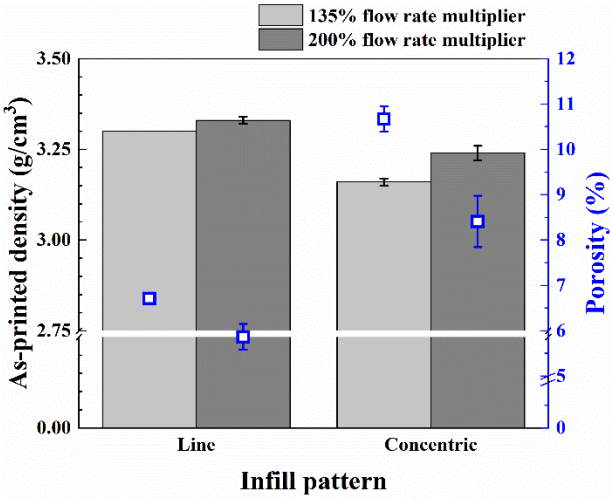

Figure 6. Effect of the extrusion multiplier on the as-printed density and porosity for specimens printed using the 0.1 mm layer thickness and 235°C printing temperature.

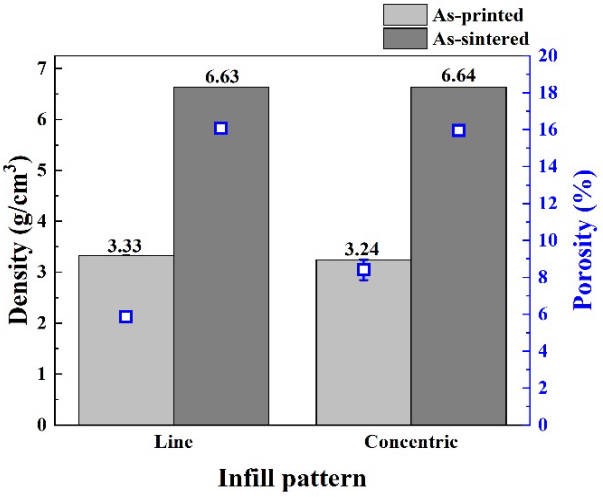

Figure 7. As-printed and as-sintered density of specimens printed with the 0.1 mm layer thickness, 235°C printing temperature and 2.0 extrusion multiplier.

3.3 As-printed and as-sintered internal structures

Figure 8 and Figure 9 show the (a) as-printed and (b) as-sintered internal structures of specimens printed with the line and concentric infill patterns as analysed by micro CT-scan respectively. There is no observable void or defect present in the as-printed specimen, printed with the line infill pattern from both front and side views (Figure 8(a)). On the other hand, for the as-printed internal structure of the specimen printed with the concentric infill pattern, some voids between deposited paths are observed (white arrows in Figure 9(a) at F-2 and S-1 positions). Similar voids, however, were not observed in the specimen printed with the line infill pattern since each infill layer was alternately printed at a 90° rotation with respect to the previous layer, and hence the gaps between deposited paths were also alternated. Therefore, the gaps between line infill deposited paths can be more readily filled than the concentric infill pattern where the gaps between deposited paths will always be in the same x-y position. This behaviour results in the specimens printed with the concentric infill pattern having slightly lower as-printed densities than those printed with the line infill pattern for all printing temperatures and layer thicknesses (Figure 5).

After sintering, for the line infill pattern in Figure 8(b), many randomly internal voids can be clearly observed especially in the infill area. This is different from that of the concentric infill pattern, in which voids between deposited paths can be clearly observed and become very pronounced (a white arrow in Figure 9(b) at the position of F-2), when compared to the as-printed specimen (Figure 9(a)). From the side view for both infill patterns, the voids are seen to be elongated, which reflects the formation of the voids that occur at the interlayer region. This suggests that the main voids inside the specimens were induced and generated from the voids between the deposited path (both between neighbouring printing paths (in the X-Y direction) and between printed layers (in the Z direction)). Similar large voids were reported elsewhere [24,25] when the commercially available metal-filled filament from the same supplier is used. This behaviour can be explained by the fusion of neighbouring metal powders to decrease the free surface energy, which results in decreasing voids between the metal powders but enlarging voids between deposited paths. Considering the relationship between as-printed and as-sintered density between both infill patterns, there is an insignificant difference between the as-sintered density of line and concentric infill patterns, which are 6.63 g·cm^{-3} to 6.64 g·cm^{-3} (~83% of relative sintered density), even though the line infill pattern has higher as-printed density. This possibly results from the formation of voids, generated during debinding of the line infill pattern specimen since there is no systematic relationship of voids between as-printed and as-sintered parts.

Table 2. Chemical composition analysed by EDS analysis in the as-sintered specimen compared with MPIF standard 35.

Elements	As-sintered specimen (wt%)	MPIF-35 (wt%) [46]
C	1.86 ± 0.19	0.07 max
Si	0.78 ± 0.06	1.0 max
P	-	0.03 max
S	0.03 ± 0.02	0.035 max
Cr	16.44 ± 0.08	15.5-17.5
Mn	0.15 ± 0.04	1.0 max
Ni	4.21 ± 0.07	3.0-5.0
Cu	3.06 ± 0.07	3.0-5.0
Nb	0.29 ± 0.07	-
Ta	0.02 ± 0.17	-
Fe	Balance	Balance

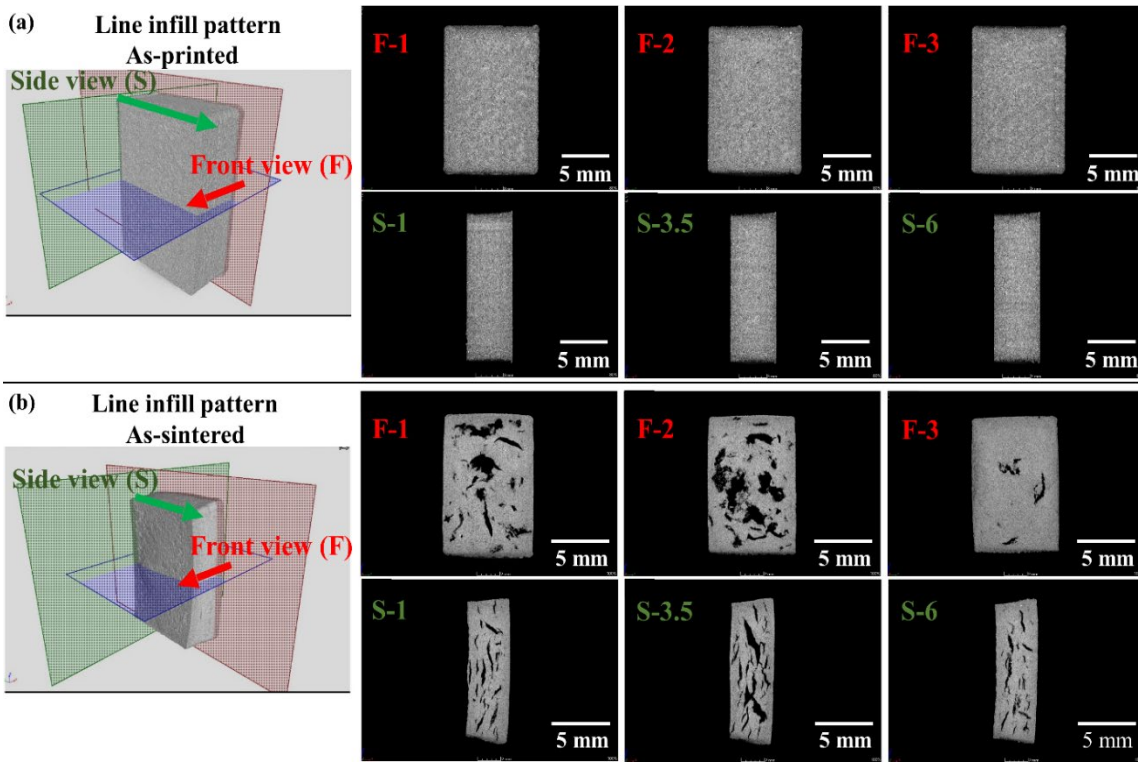

Figure 8. The front (F) and side views (S) of the paused layer, observed from the micro-CT scans at different positions for (a) as-printed, and (b) as-sintered specimens, printed with the line infill pattern. The number after F and S represents the paused position away from the origin point in the unit of mm. Noted that the as-printed and as-sintered results were scanned from the different specimens.

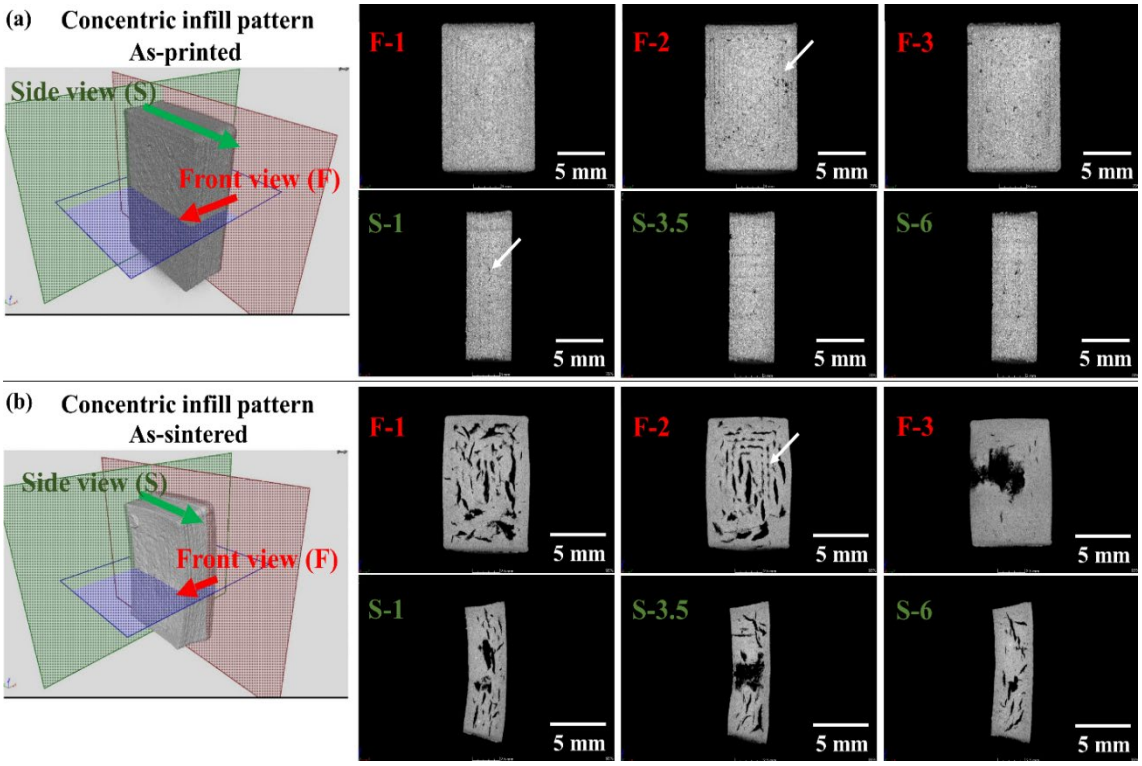

Figure 9. The front (F) and side views (S) of the paused layer, observed from the micro-CT scans at different positions for (a) as-printed, and (b) as-sintered specimens, printed with the concentric infill pattern. The number after F and S represents the paused position away from the origin point in the unit of mm. Noted that the as-printed and as-sintered results were scanned from the different specimens.

3.4 Macro- and microstructures

The chemical composition of the as-sintered specimen, analysed by EDS, is presented in Table 2, together with the Metal Powder Industries Federation (MPIF) Standard 35 for metal injection molding materials. The chemical composition aligns well with the MPIF-35 standard. However, inaccuracies in the C content may be expected due to its low atomic number.

The comparison of XRD diffraction patterns between powder and the as-sintered specimen, shown in Figure 10, shows the similar major phase of ferrite (α) and/or martensite (α'). It is known that the major phase of 17-4PH is more likely to be martensite than ferrite because the martensite finish transformation temperature (32°) is higher than room temperature [41,42]. However, it cannot be differentiated between these two structures by XRD, including delta-ferrite [43-45] since the crystal structure of martensite (α' bct) is very close to that of ferrite (bcc α).

The macro- and microstructures of cross-sections of the as-sintered specimen, having the highest as-sintered density, printed with 235°C printing temperature, 0.1 mm layer thickness and 2.0 extrusion multiplier by using the concentric infill pattern are presented in Figure 11. The macrograph in Figure 11(a) shows large voids similar to those observed by micro-CT scanning in Figure 9(b). At higher magnification (Figure 11(b)), the voids exhibit incomplete bonding behaviour of the matrix. This behaviour may have resulted from (i) the voids between deposited paths (a white arrow in Figure 9(a) at the position of F-2) and (ii) too low solid loading of the powder in the filament. As reported in Section 3.1, the solid loading of powder in the metal-filled filament is 77 wt%, which is noticeably lower than conventional solid loading (more than 90 wt%) [7,13,47-49]. Figure 11(c) shows the porosity that stems from the nature of pressureless sintering. The microstructure of the specimen, shown in Figure 11(d), well agrees with the XRD analysis composing martensite and/or ferrite. Delta-ferrite along the grain boundary is also observed, confirmed by Cr-rich area in EDS elemental mapping, shown in Figure 12. This pattern is similar to what has been reported in 17-4PH stainless steel fabricated by MIM process [50]. In addition, a Si-O-rich phase seen as dark grey particles was also observed as confirmed by the EDS elemental mapping shown in Figure 12. This is consistent with SiO_2 as typically found in 17-4PH fabricated by the MIM process [50]. The formation of SiO_2 in MIM parts results from the formation of SiO_2 at the surface of the powder since the water atomisation [4].

3.5 Tensile properties

Figure 13 shows (a) the overall shape of as-printed and as-sintered tensile test specimens, and (b) the representative stress vs strain curves of 17-4PH specimens printed with the printing parameters of 235°C printing temperature, 0.1 mm layer thickness, 2.0 extrusion multiplier with different infill patterns. The sintered tensile test specimen in Figure 13(a) significantly shrank (~12-15%) compared with the as-printed specimen but the overall shape was retained. From the visualisation, there is no external defect. It was found that the tensile strength of the specimen printed with the concentric infill pattern (~325 MPa) is significantly higher than the line infill pattern (~180 MPa). This possibly results from the orientation of the voids to the load direction, in which the specimen printed with the concentric infill pattern exhibits parallel voids to the load direction. On the other hand, for the specimen printed with the line infill pattern, the voids are at angle to the load direction. The elongation of both specimens is comparable. The tensile strength and elongation of both infill patterns are significantly lower than those obtained using other 17-4PH filaments with higher solid loading and no internal defects after sintering. It is noted that many attempts were applied to obtain defect-free tensile specimens but it was not possible using the filament in this study. Similarly, it is not possible to obtain defect-free tensile sample for the CuSi12 filament from the sample supplier and the tensile properties are lower than expected [24,25].

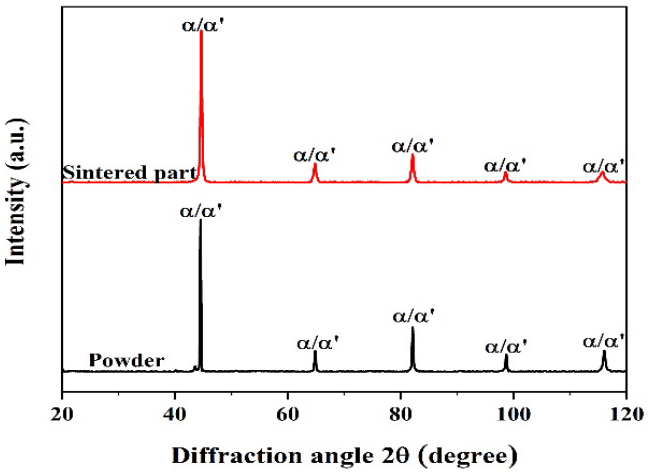

Figure 10. XRD diffraction patterns of 17-4PH powder and sintered specimen.

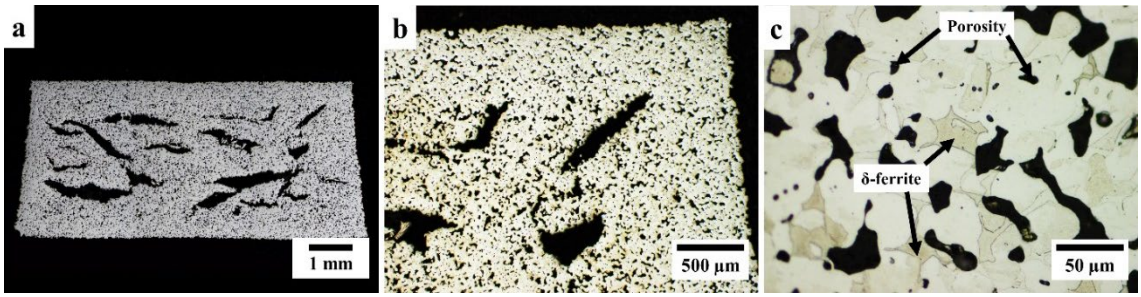

Figure 11. Macro-and microstructures of the highest as-sintered specimen (corresponding to Figure 9(b)) - (a) overall cross-section, (b) high magnification, showing large voids, and (c) high magnification, showing typical porosity from the pressureless sintering process and δ-ferrite structure.

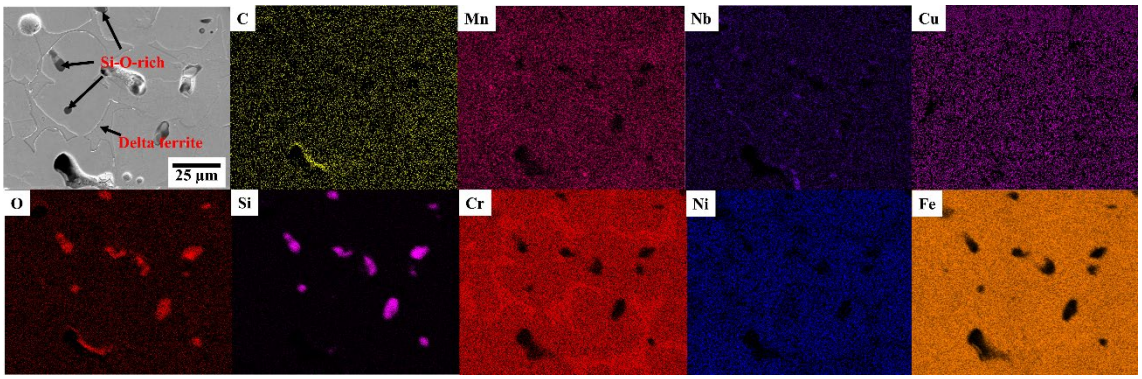

Figure 12. SEM micrograph and related EDS elemental mapping of as-sintered specimens, showing the Si-O-rich particle with Cr-rich area along the grain boundary.

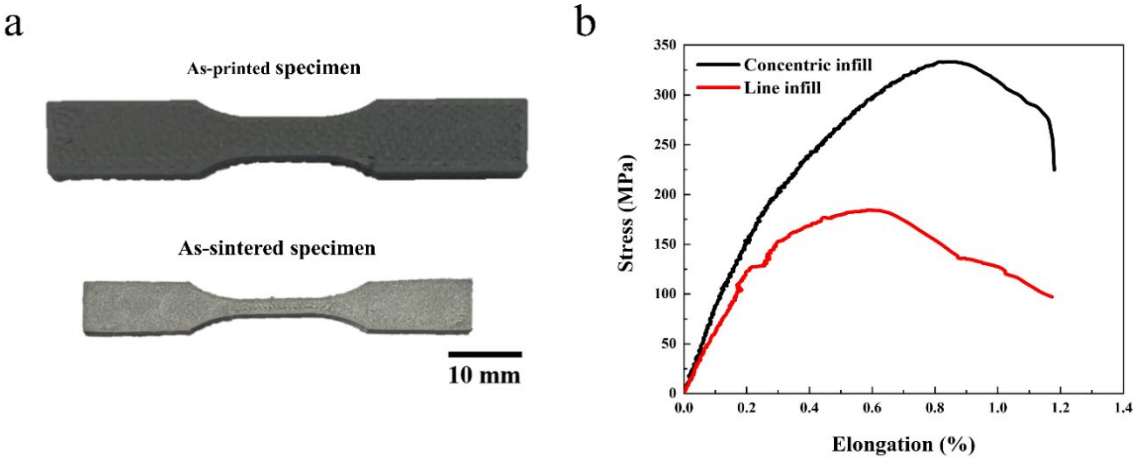

Figure 13. (a) A photograph of as-printed and as-sintered tensile test specimens with the line infill pattern, and (b) representative stress vs strain curves of 17-4PH specimens printed using the optimum condition (235°C printing temperature, 0.1 mm layer thickness, 2.0 extrusion multiplier) with different infill patterns.

4. Conclusions

In the present study, the 17-4PH stainless steel metal-filled filament was characterised and the effects of printing parameters, layer thickness, infill pattern and extrusion multiplier were studied. The key conclusions are as follows:

1. The filament composes of at least two main components of binder and 77 wt% metal powder, which is lower than conventional solid loadings from the literature (more than 90%). This could potentially generate internal voids after sintering.
2. All printing parameters in the present study significantly influenced the density of the as-printed specimen. However, the as-sintered densities of both infill patterns are insignificantly different.
3. Although there is no external defect of the tensile specimen, there is still an internal defect that contributes to unexpected low tensile properties and causes the difference in tensile properties between the specimens printed with concentric and line infill patterns.

Acknowledgements

This work is financially supported by National Metal and Materials Technology Center (MTEC) and Septillion Co., Ltd., Thailand (Grant No. P1952439). The authors would like to sincerely thank Septillion Co., Ltd., Thailand for the support of the FFF printer, and Dr. John T.H. Pearce, Department of Industrial Chemistry, Chiang Mai University, Thailand for valuable discussions and proofreading.

References

[1] D. Barba, C. Alabort, Y. T. Tang, M. J. Viscasillas, R. C. Reed, and E. Alabort, "On the size and orientation effect in additive manufactured Ti-6Al-4V," *Materials & Design,* vol. 186, p. 108235, 2020.

[2] R. A. Michi, A. Plotkowski, A. Shyam, R. R. Dehoff, and S. S. Babu, "Towards high-temperature applications of aluminium alloys enabled by additive manufacturing," *International Materials Reviews,* pp. 1-48, 2021.

[3] T. DebRoy, H. L. Wei, J. S. Zuback, T. Mukherjee, J. W. Elmer, J. O. Milewski, A. M. Beese, A. Wilson-Heid, A. De, and W. Zhang, "Additive manufacturing of metallic components – Process, structure and properties," *Progress in Materials Science,* vol. 92, pp. 112-224, 2018.

[4] W. E. Frazier, "Metal additive manufacturing: A review," *Journal of Materials Engineering and Performance,* vol. 23, no. 6, pp. 1917-1928, 2014.

[5] I. Thawon, T. Fongsamootr, Y. Mona, and P. Suttakul, "Investigation of the mechanical properties of additively manufactured metal parts with different relative densities," *Applied Sciences,* vol. 12, no. 19, p. 9915, 2022.

[6] J. Gonzalez-Gutierrez, S. Cano, S. Schuschnigg, C. Kukla, J. Sapkota, and C. Holzer, "Additive manufacturing of metallic and ceramic components by the material extrusion of highly-filled polymers: A review and future perspectives," *Materials,* vol. 11, no. 5, p. 840, 2018.

[7] C. Suwanpreecha, and A. Manonukul, "A review on material extrusion additive manufacturing of metal and how it compares with metal injection moulding," *Metals,* 2022.

[8] S. Riecker, J. Clouse, T. Studnitzky, O. Andersen, and B. Kieback, "Fused deposition modeling-opportunities for cheap metal AM," *World PM2016-AM-Deposition Technologies,* 2016.

[9] H. Gong, D. Snelling, K. Kardel, and A. Carrano, "Comparison of stainless steel 316L parts made by FDM- and SLM-based additive manufacturing processes," *JOM,* vol. 71, no. 3, pp. 880-885, 2019.

[10] D. Godec, S. Cano, C. Holzer, and J. Gonzalez-Gutierrez, "Optimization of the 3D printing parameters for tensile properties of specimens produced by fused filament fabrication of 17-4PH stainless steel," *Materials,* vol. 13, no. 3, p. 774, 2020.

[11] M. Á. Caminero, A. Romero, J. M. Chacón, P. J. Núñez, E. García-Plaza, and G. P. Rodríguez, "Additive manufacturing of 316L stainless-steel structures using fused filament fabrication technology: Mechanical and geometric properties," *Rapid Prototyping Journal,* 2021.

[12] Y. Wang, L. Zhang, X. Li, and Z. Yan, "On hot isostatic pressing sintering of fused filament fabricated 316L stainless steel – evaluation of microstructure, porosity, and tensile properties," *Materials Letters,* p. 129854, 2021.

[13] M. Quarto, M. Carminati, and G. D'Urso, "Density and shrinkage evaluation of AISI 316L parts printed via FDM process," *Materials and Manufacturing Processes,* pp. 1-9, 2021.

[14] M. A. Wagner, A. Hadian, T. Sebastian, F. Clemens, T. Schweizer, M. Rodriguez-Arbaizar, E. Carreño-Morelli, and R. Spolenak, "Fused filament fabrication of stainless steel structures - from binder development to sintered properties," *Additive Manufacturing,* p. 102472, 2021.

[15] C. Suwanpreecha, and A. Manonukul, "On the build orientation effect in as-printed and as-sintered bending properties of 17-4PH alloy fabricated by metal fused filament fabrication," *Rapid Prototyping Journal,* vol. ahead-of-print, no. ahead-of-print, 2022.

[16] C. Suwanpreecha, P. Seensattayawong, V. Vadhanakovint, and A. Manonukul, "Influence of specimen layout on 17-4PH (AISI 630) alloys fabricated by low-cost additive manufacturing," *Metallurgical and Materials Transactions A,* 2021.

[17] J. Gonzalez-Gutierrez, F. Arbeiter, T. Schlauf, C. Kukla, and C. Holzer, "Tensile properties of sintered 17-4PH stainless steel fabricated by material extrusion additive manufacturing," *Materials Letters,* vol. 248, pp. 165-168, 2019.

[18] Y.-H. Cho, S.-Y. Park, J.-Y. Kim, and K.-A. Lee, "17-4PH stainless steel with excellent strength–elongation combination developed via material extrusion additive manufacturing," *Journal of Materials Research and Technology,* vol. 24, pp. 3284-3299, 2023.

[19] Y. Abe, T. Kurose, M. V. Santos, Y. Kanaya, A. Ishigami, S. Tanaka, and H. Ito, "Effect of layer directions on internal structures and tensile properties of 17-4PH stainless steel parts fabricated by fused deposition of metals," *Materials,* vol. 14, no. 2, p. 243, 2021.

[20] J. A. Naranjo, C. Berges, A. Gallego, and G. Herranz, "A novel printable high-speed steel filament: Towards the solution for wear-resistant customized tools by AM alternative," *Journal of Materials Research and Technology,* vol. 11, pp. 1534-1547, 2021.

[21] Y. Thompson, M. Polzer, J. Gonzalez-Gutierrez, O. Kasian, J. P. Heckl, V. Dalbauer, C. Kukla, and P. J. Felfer, "Fused filament fabrication-based additive manufacturing of commercially pure titanium," *Advanced Engineering Materials*, vol. 23, no. 12, p. 2100380, 2021.

[22] Z. Lu, O. I. Ayeni, X. Yang, H.-Y. Park, Y.-G. Jung, and J. Zhang, "Microstructure and phase analysis of 3D-printed components using bronze metal filament," *Journal of Materials Engineering and Performance,* vol. 29, no. 3, pp. 1650-1656, 2020.

[23] J. Gonzalez-Gutierrez, S. Cano, J. V. Ecker, M. Kitzmantel, F. Arbeiter, C. Kukla, and C. Holzer, "Bending properties of lightweight copper specimens with different infill patterns produced by material extrusion additive manufacturing, solvent debinding and sintering," *Applied Sciences,* vol. 11, no. 16, p. 7262, 2021.

[24] X. Wei, I. Behm, T. Winkler, S. Scharf, X. Li, and R. Bähr, "Experimental study on metal parts under variable 3D printing and sintering orientations using bronze/PLA hybrid filament coupled with fused filament fabrication," *Materials,* vol. 15, no. 15, p. 5333, 2022.

[25] B. Aruanno, A. Paoli, A. V. Razionale, and F. Tamburrino, "Effect of printing parameters on extrusion-based additive manufacturing using highly filled CuSn12 filament," *The International Journal of Advanced Manufacturing Technology,* pp. 1-14, 2023.

[26] P. Singh, V. K. Balla, A. Gokce, S. V. Atre, and K. H. Kate, "Additive manufacturing of Ti-6Al-4V alloy by metal fused filament fabrication (MF3): producing parts comparable to that of metal injection molding," *Progress in Additive Manufacturing,* vol. 6, no. 5, 2021.

[27] P. Singh, V. K. Balla, S. V. Atre, R. M. German, and K. H. Kate, "Factors affecting properties of Ti-6Al-4V alloy additive manufactured by metal fused filament fabrication," *Powder Technology,* vol. 386, pp. 9-19, 2021.

[28] Y. Zhang, S. Bai, M. Riede, E. Garratt, and A. Roch, "A comprehensive study on Fused filament fabrication of Ti-6Al-4V structures," *Additive Manufacturing,* p. 101256, 2020.

[29] P. Singh, V. K. Balla, A. Tofangchi, S. V. Atre, and K. H. Kate, "Printability studies of Ti-6Al-4V by metal fused filament fabrication (MF3)," *International Journal of Refractory Metals and Hard Materials,* vol. 91, p. 105249, 2020.

[30] G. Kiswanto, A. Kholil, and J. Istiyanto, "Effect of infill pattern on impact toughness, microstructure, and surface roughness of inconel 625 built via filament-based material extrusion additive manufacturing," *Journal of Manufacturing and Materials Processing,* vol. 7, no. 3, p. 114, 2023.

[31] Y. Thompson, K. Zissel, A. Förner, J. Gonzalez-Gutierrez, C. Kukla, S. Neumeier, and P. Felfer, "Metal fused filament

fabrication of the nickel-base superalloy IN 718," *Journal of Materials Science,* pp. 1-15, 2022.

[32] "Ultrafuse 316L, https://www.ultrafusefff.com/product-category/metal/ultrafuse-316l/ (accessed on 27 October 2021)."

[33] "The virtual foundry, printing pure metal with filamet™, https:// www. thevirtualfoundry.com/help, (accessed on 27 October 2021)."

[34] M. Q. Shaikh, P.-Y. Lavertu, K. H. Kate, and S. V. Atre, "Process sensitivity and significant parameters investigation in metal fused filament fabrication of Ti-6Al-4V," *Journal of Materials Engineering and Performance,* vol. 30, no. 5, pp. 5118-5138, 2021.

[35] T. Kurose, Y. Abe, M. V. Santos, Y. Kanaya, A. Ishigami, S. Tanaka, and H. Ito, "Influence of the layer directions on the properties of 316L stainless steel parts fabricated through fused deposition of metals," *Materials,* vol. 13, no. 11, p. 2493, 2020.

[36] W. Hassan, M. A. Farid, A. Tosi, K. Rane, and M. Strano, "The effect of printing parameters on sintered properties of extrusion-based additively manufactured stainless steel 316L parts," *The International Journal of Advanced Manufacturing Technology,* vol. 114, no. 3, pp. 1-11, 2021.

[37] G. Singh, J.-M. Missiaen, D. Bouvard, and J.-M. Chaix, "Copper extrusion 3D printing using metal injection moulding feedstock: Analysis of process parameters for green density and surface roughness optimization," *Additive Manufacturing,* vol. 38, p. 101778, 2021.

[38] T. Rosnitschek, A. Seefeldt, B. Alber-Laukant, T. Neumeyer, V. Altstädt, and S. Tremmel, "Correlations of geometry and infill degree of extrusion additively manufactured 316L stainless steel components," *Materials,* vol. 14, no. 18, p. 5173, 2021.

[39] A. S. f. Testing and Materials, "B962-17: standard test methods for density of compacted or sintered Powder Metallurgy (PM) products using archimedes' principle," 2019: ASTM West Conshohocken.

[40] K. Gante Lokesha Renukaradhya, "Metal filament 3D printing of SS316L: Focusing on the printing process," ed, 2019.

[41] A. Bhaduri, S. Sujith, G. Srinivasan, T. Gill, and S. Mannan, "Optimized postweld heat treatment procedures for 17-4 PH stainless steels," Welding Journal, vol. 74, no. 5, p. 153, 1995.

[42] J. R. Davis, *Stainless steels*. ASM international, 1994.

[43] P. Suri, B. Smarslok, and R. M. German, "Impact properties of sintered and wrought 17–4 PH stainless steel," *Powder metallurgy,* vol. 49, no. 1, pp. 40-47, 2006.

[44] R. Schroeder, G. Hammes, C. Binder, and A. N. Klein, "Plasma debinding and sintering of metal injection moulded 17-4PH stainless steel," *Materials Research,* vol. 14, pp. 564-568, 2011.

[45] R. J. Hamlin and J. N. DuPont, "Microstructural evolution and mechanical properties of simulated heat-affected zones in cast precipitation-hardened stainless steels 17-4 and 13-8+ Mo," *Metallurgical and Materials Transactions A,* vol. 48, no. 1, pp. 246-264, 2017.

[46] MPIF, "Material standards for metal injection molded parts," *Princeton, NJ, Metal Powder Industries Federation.* 2016.

[47] G. Singh, J.-M. Missiaen, D. Bouvard, and J.-M. Chaix, "Additive manufacturing of 17-4 PH steel using metal injection moulding feedstock: analysis of 3D extrusion printing, debinding and sintering," *Additive Manufacturing,* p. 102287, 2021.

[48] M. Sadaf, M. Bragaglia, and F. Nanni, "A simple route for additive manufacturing of 316L stainless steel via Fused filament fabrication," *Journal of Manufacturing Processes,* vol. 67, pp. 141-150, 2021.

[49] D. Jiang and F. Ning, "Additive manufacturing of 316L stainless steel by a printing-debinding-sintering method: effects of microstructure on fatigue property," *Journal of Manufacturing Science and Engineering,* pp. 1-30, 2021.

[50] M.-W. Wu, Z.-K. Huang, C.-F. Tseng, and K.-S. Hwang, "Microstructures, mechanical properties, and fracture behaviors of metal-injection molded 17-4PH stainless steel," *Metals and Materials International,* vol. 21, no. 3, pp. 531-537, 2015.